Ultrasound in Med. & Biol., Vol. 27, No. 12, pp. 1677–1682, 2001

0301-5629/01/$–see front matter

PII: S0301-5629(01)00472-0

● *Original Contribution*

EXPERIMENTAL CORROBORATION OF THE NONSTATIONARY STRAIN ESTIMATION ERRORS IN ELASTOGRAPHY

TOMY VARGHESE* and JONATHAN OPHIR†

*Department of Medical Physics, The University of Wisconsin-Madison, Madison, WI, USA; and †Department of Radiology, Ultrasonics Laboratory, The University of Texas Medical School, Houston, TX, USA

(*Received* 20 *March* 2001; *in final form* 17 *September* 2001)

Abstract—The nonstationary variation in the noise performance of the cross-correlation-based strain estimator due to frequency-dependent attenuation and lateral and elevational signal decorrelation have been addressed theoretically in recent papers using the strain-filter approach. In this paper, we present the experimental verification and corroboration of the nonstationary effects on the strain estimation results. The accuracy and precision of the strain estimate deteriorates with lateral position in the elastogram, due to the lateral motion of tissue scatterers, and with depth, due to frequency-dependent attenuation. The results illustrate that the best strain-estimation noise performance is obtained in the focal zone of the transducer and around the axis of symmetry of the phantom. (E-mail: tvarghese@facstaff.wisc.edu) © 2002 World Federation for Ultrasound in Medicine & Biology.

Key Words: **Ultrasound, Strain, Imaging, Cross-correlation, Dynamic range, Elastography, Elastogram, Strain filter.**

INTRODUCTION

Elastography, a method for imaging the elastic properties of compliant tissues, was proposed by Ophir et al. (1991). In this imaging modality, tissue stiffnesses are visualized using grey-scale strain images referred to as elastograms (Ophir et al. 1991, 1999). Significant research has been devoted to the imaging of elastic parameters of soft tissue (Bamber and Bush 1996; Céspedes 1993; de Korte et al. 1997; Garra et al. 1997; Gao et al. 1996; Krouskop et al. 1987; O'Donnell et al. 1991; Ophir et al. 1991, 1999; Parker et al. 1990; Wilson and Robinson 1982; Yamakoshi et al. 1990). Elastography has been successfully applied *in vivo* for breast cancer evaluation and has shown great potential for improving the ability of radiologists to distinguish benign from malignant masses (Garra et al. 1997).

The elastographic system has been characterized using both theoretical (Varghese and Ophir 1997a; Varghese et al. 1998) and experimental (Varghese and Ophir 1999) methods. The general theoretical framework, referred to as the strain filter (SF) (Varghese and Ophir 1997a), describes the relationship among the resolution, dynamic range, sensitivity and elastographic SNR (SNR_e). The SF may be plotted as a graph of the upper bound of the SNR_e vs. the strain experienced by the tissue, for a given elastographic axial resolution as determined by the data window length and overlap (Alam et al. 2000). The SF may be derated, due to effects such as tissue attenuation (Varghese and Ophir 1997b) and speckle decorrelation, due to undesired lateral tissue motion (Kallel et al. 1997).

Estimation of tissue strains is inherently a nonstationary process because the pre- and postcompression radiofrequency (RF) echo signals are jointly nonstationary (due to signal deformation caused by straining tissue). However, the pre- and postcompression signals can be assumed to be jointly stationary, if the tissue strain is estimated using small windowed data segments in conjunction with temporal stretching of the postcompression signal. Frequency-dependent attenuation introduces additional (axial) nonstationarity into the strain estimation process vs. depth (Varghese and Ophir 1997b), and lateral and elevational signal decorrelation introduce nonstationarities in the strain estimation process along the lateral and elevational directions, respectively (Kallel et al. 1997). The SF can predict the effect of these nonstationarities on the elastogram.

The next section presents the experimental setup

Address correspondence to: Dr. Tomy Varghese, Department of Medical Physics, The University of Wisconsin-Madison, Madison, WI 53706 USA. E-mail: tvarghese@facstaff.wisc.edu

used in the verification and corroboration of the nonstationary behavior with depth and lateral position of the SF concept. The derating of the SF that occurs due to frequency-dependent attenuation and lateral decorrelation is demonstrated in the section following the discussion of the setup. Finally, the Conclusion section summarizes the contributions of this paper.

EXPERIMENTAL SETUP

The ultrasound (US) system used for elastography is a Diasonics Spectra II real-time scanner (Diasonics Inc., Santa Clara, CA) operating with dynamic receive focusing and a single transmit focus centered at a depth of 3 cm. The transducer characterized is a 100-element linear-array (40 mm) with a 5-MHz center frequency (f-number = 20.4 mm^{-1}) and a 60% bandwidth. The beamwidth of the transducer was 1.5 mm with a corresponding pitch 0.4 mm. The digitizer used is an 8-bit digitizer (LeCroy Corp., Spring Valley, NY) operating at 48 MHz. The digitized data were collected from a 40 $\times$ 50 mm region-of-interest (ROI) consisting of 100 A-lines (starting at a depth of 5 mm under the transducer) centered around the transmit focus. The system also includes a motion control system, and a compression device. A personal computer controls the operation of the entire system. A complete description of the elastography system was presented by Céspedes (1993).

Method

The tissue-mimicking ultrasonic and elastographic phantom (70 $\times$ 70 $\times$ 90 mm) was constructed from water-based gels (Hall et al. 1997). The phantom contains scatterers (graphite flakes) and was used to obtain RF scans before and after compression. A large compressor was used to simulate uniform stress conditions in the phantom. In addition, we attempted to create perfect slip boundary conditions by lubricating both the upper and lower surfaces of the phantom with corn oil.

The pre- and postcompression RF scans of the uniformly elastic phantom were obtained for compressions ranging from 0.1% to 15% at depths of 0.5 cm to 5.5 cm. The transducer focal region in the phantom is at a depth between 2.5 and 3.5 cm. The entire experiment was repeated 25 times to obtain independent realizations of the signals. To obtain uncorrelated data sets, the following procedures were performed individually: the transducer was moved in small increments (greater than the lateral beamwidth) in the lateral direction; the phantom was rotated about its axis; and small changes were made in the precompression of the phantom. All the generated data were stored for off-line processing. The 25 data sets collected in the experiment allowed the use of statistical methods to analyze the noise performance of the strain-estimation process.

The strain estimates were obtained from the gradient of the displacement estimates computed using 3-mm windowed data segments (Z) with a 50% overlap between the successive data segments. The pre- and stretched postcompression RF echo signals were zero-padded to reduce the effects of time-domain aliasing. The 25 strain estimates obtained were sorted and five outliers were eliminated, to avoid biasing the strain estimates by either high or low strain values. The means and SD of the remaining 20 strain estimates were calculated, and the elastographic SNR_e at each applied strain level was computed. Because we used a uniformly elastic phantom, the applied strain equalled the internal strain generated in the phantom. This process was repeated for all the applied strains, to generate the experimental strain filter (ESF) (Varghese and Ophir 1999).

Estimation of parameters from the experimental data for the SF

The sonographic SNR (SNR_S) of the pre- and postcompression signals obtained by insonifying the elastographic phantom is required to compute the corresponding SF. The SNR_S in the RF signal was computed at the focus of the transducer and under the assumption that the noise in the signals can be modeled as white noise. The SNR_S of the RF echo signal was computed from the expected value of the Fourier power spectrum. The expected value of the power spectrum for the specified window length was computed from the ensemble of RF signals at the same location in the elastographic phantom. We obtained an estimate of the average signal and noise power around the center frequency of the transducer, and an estimate of the average noise power. The signal and noise regions used to compute the SNR_S are illustrated in Fig. 1. The average noise power was subtracted from the estimate of the average signal and noise obtained near the transducer center frequency. The ratio of the signal estimate to the noise estimate determines the SNR_S of the signal. Computing the SNR_S in this manner lead to a value of 28.4 dB for the RF echo signals. This value of the SNR_S was used in the computation of the corresponding theoretical SF for comparison with the estimated ESF. The noise calculations were based on the assumption of white noise in the RF signal.

Because the ESF at every other position in the elastogram depends on the attenuation of the elastographic phantom, in addition to other factors, such as the boundary conditions and lateral and elevational signal decorrelation, the value of the attenuation coefficient must be known to compute the variation in the ESF with depth. The attenuation coefficient in the phantom was estimated from the slope of the straight line fit to the log ratio of spectra at two depths (Parker et al. 1988), and using the shift in the center frequency with depth (Parker

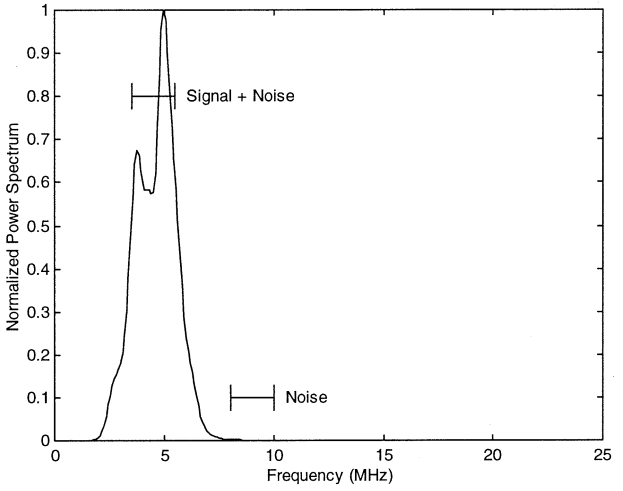

Fig. 1. Computation of the SNR_S in the RF signal from the expected value of the power spectrum. The signal and noise regions in the power spectrum are shown.

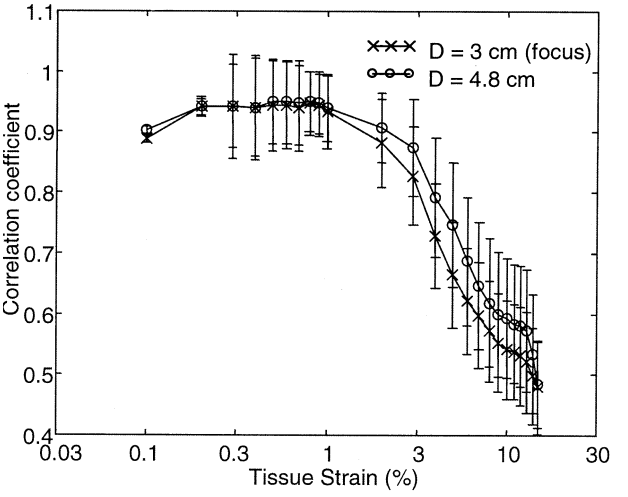

Fig. 2. The correlation coefficient between the pre- and post-compression echo signals at the focus 3 cm (×), and at a depth of 4.8 cm (○).

et al. 1988) to obtain the SF corresponding to the ESF at different depths in the phantom. The attenuation coefficient was estimated to have a value of 0.59 dB/cm MHz, corresponding to a shift in the center frequency of 0.393 MHz/cm.

EXPERIMENTAL CORROBORATION OF THE NONSTATIONARY BEHAVIOR

The ESF obtained depends on the properties of the elastographic phantom used. The attenuation in the phantom significantly impacts the precision of the strain estimates, due to downshift in the center frequency and the bandwidth. In addition, the motion of the scatterers in the lateral and elevational directions (away from the axis of symmetry) increases signal decorrelation effects, thereby reducing the precision of the strain estimates. The changes in the ESF with depth and lateral position are discussed and compared to the SF derated for these effects in this section.

The nonstationary variation in the ESF with depth

Additional errors in the strain estimates caused by frequency-dependent attenuation are evaluated using the ESF in this section. This analysis was performed for the RF A-line along the axis of the transducer, to minimize the effects of lateral signal decorrelation and beam effects. The mean correlation coefficient estimates at three depths within the phantom are illustrated in Fig. 2. Note that the mean correlation coefficient estimates away from the focus (at 4.8 cm) are lower than the estimates obtained in the focal zone. The results in Fig. 2 also indicate that the mean correlation coefficient estimates near the far-field are higher than those in the focal zone for large strains (due to the center-frequency downshift with depth). This result contributes to the movement of the SF (Varghese and Ophir 1997b) and of the ESF toward larger strains with increased depth in the phantom. The center frequency downshift due to frequency-dependent attenuation reduces the higher frequencies in the signal, thereby improving the value of the correlation coefficient and, hence, the strain estimation SNR_e, as illustrated in Figs. 3 and 4 at higher strains.

The ESFs at different depths in the phantom are illustrated in Fig. 4, with the corresponding SFs illustrated in Fig. 3, computed at the SNR_S value obtained as discussed in the methods section. In addition, the derated

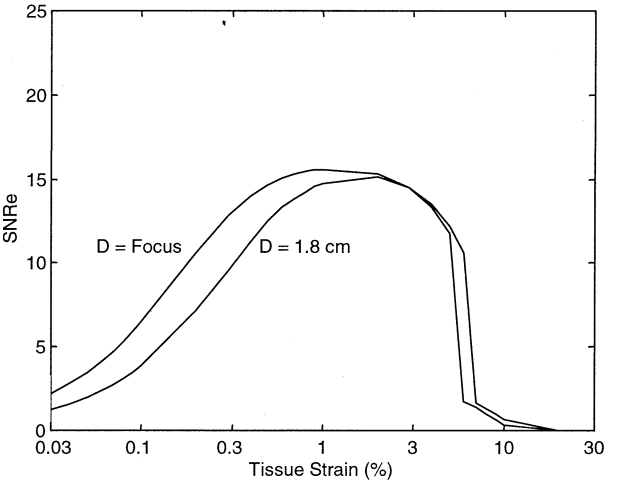

Fig. 3. The SFs obtained at the focus and at a depth of 1.8 cm.

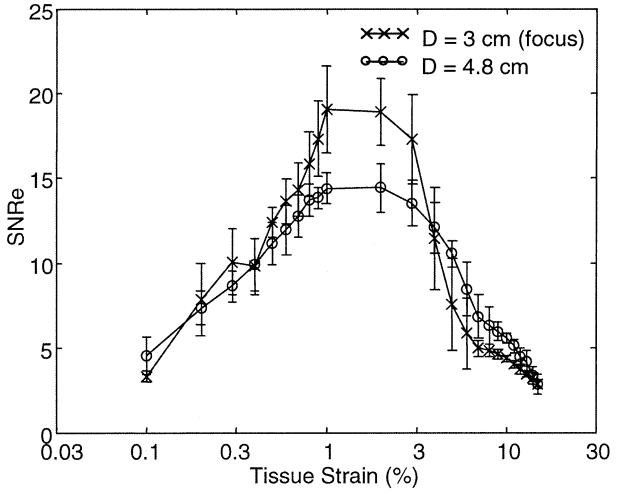

Fig. 4. The ESF obtained at different depths in the elastographic phantom. The strain estimates were made using a window length (Z) of 3 mm with a 50% overlap between data segments. Note that the ESF estimated around the focus between 2 and 3 cm is significantly better than the ESF estimated between 4.5 cm to 5.5 cm away from the focus. The nonstationary variation in the precision of the strain estimates with depth is illustrated using the ESF.

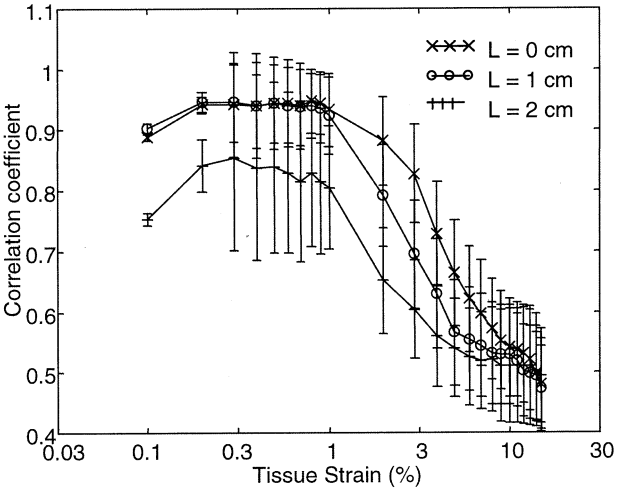

Fig. 5. The correlation coefficient between the pre- and post-compression echo signals at a lateral positions of 0, 1 and 2 cm, respectively.

SF in Fig. 3 is obtained by reducing the SNR_S using the attenuation coefficient value in the phantom, as discussed in the Methods section. Note that the ESF estimated in the focal zone is significantly higher than the ESF estimated away from the focus (between 4.5 cm to 5.5 cm). The contributions of frequency-dependent attenuation can be observed when comparing the ESF in the focal zone and the far-field, respectively. Note the reduction in the sensitivity and in the maximum SNR_e value due to the corresponding reduction in the SNR in the RF signals. The movement of the ESF toward larger strains with depth in the phantom due to the center frequency downshift is also clearly illustrated in Fig. 4.

The nonstationary variation in the ESF with lateral position

Reduction in the elastographic SNR_e with lateral position, predicted using the SF formulation, has been validated experimentally by Kallel and Ophir (1997). However, the ESFs at different lateral positions in the elastogram were not generated. The SNR_e in the elastogram is maximized when the US beam is on the axis of symmetry of the target (zero lateral displacement), and decreases with an increase in lateral beam position, as discussed previously in the Method section.

The SNR_e in the elastogram reduces along the lateral direction, due to the nonstationarity in the echo signals caused by lateral signal decorrelation. To maintain a constant SNR_e in the entire elastogram, techniques to minimize the lateral motion of the tissue scatterers and, hence, lateral decorrelation are of paramount importance. Confining tissue along the lateral direction (Kallel et al. 1997) is one such technique that reduces lateral motion of the tissue scatterers; however, the elevational tissue motion (out-of-plane motion) is doubled. Reduction in the errors due to lateral motion may also obtained by tracking speckle motion along the lateral direction (while confining elevationally) proposed by Chaturvedi et al. (1998) using the SAD (sum-of-absolute-differences) algorithm used by Bohs and Trahey (1991) for blood flow estimation, or by using interpolation and recorrelation schemes as proposed by Konofagou and Ophir (1998).

Under the conditions discussed in the Method section, lateral signal decorrelation is the primary contributor to the nonstationary variation in the strain estimates, with the transducer on the axis of symmetry of the phantom. The contribution of lateral motion of the tissue scatterers is illustrated in the plots of the mean correlation coefficient estimate for different lateral positions in Fig. 5. The mean correlation coefficient estimate at $L = 0$ is obtained from data segments in the focal zone of the A-line at the center of the scan (A-line 50). This region corresponds to the scatterers that reside around the phantom's axis of symmetry, where the lateral motion is minimized. Under these conditions, only axial signal decorrelation contributes to the decrease of the measured correlation coefficient with tissue strain. Note that, with an increase in the lateral position for $L = 1$ cm (A-line 75) and 2 cm (A-line 100), the value of the correlation coefficient reduces, especially at large strains. Increased

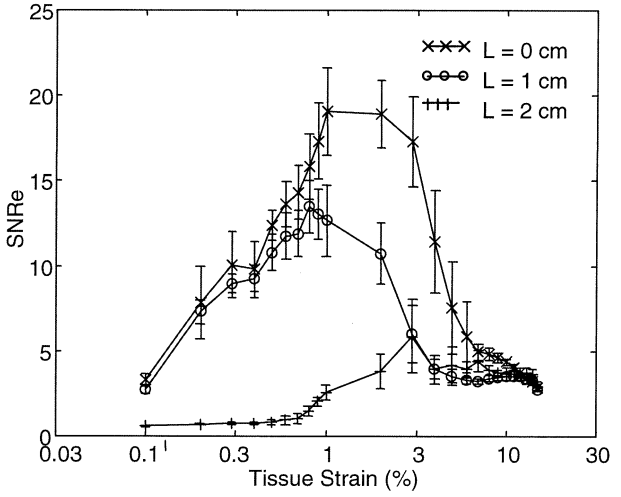

Fig. 6. The ESF estimated at different lateral positions in the elastographic phantom at the focus of the transducer. The strain estimates were made using a window length (Z) of 3 mm with a 50% overlap between data segments. Note that the ESF estimated at the center of the transducer at (L = 0 cm) is significantly better than the ESFs estimated at 1 and 2 cm. The deterioration in the precision of the strain estimates is due to the effects of lateral signal decorrelation caused due to the out-of-plane movement of the scatterers.

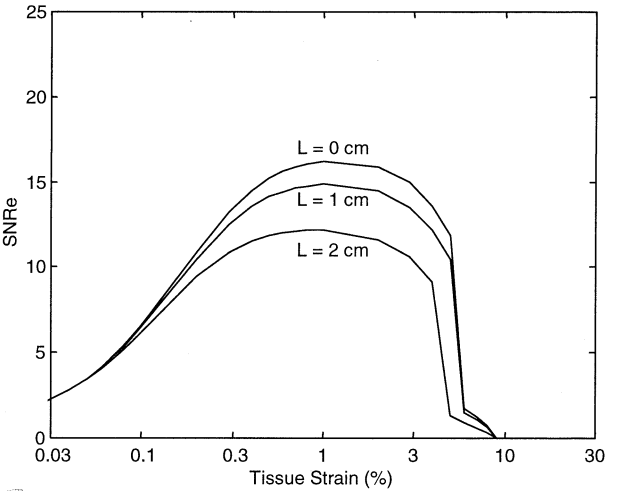

Fig. 7. The theoretical SFs obtained at lateral positions of 0, 1 and 2 cm, respectively.

tissue strains cause the tissue scatterers to move out of the US beam. In addition, the correlation coefficient obtained at 2 cm is further degraded because the effective aperture is reduced near the transducer edges.

The ESFs in the focal zone of the transducer at different lateral positions in the elastogram in Fig. 6 illustrate the nonstationary variation in the elastographic SNR_e. Note that the ESF estimated at the center of the transducer at L = 0 cm (no lateral signal decorrelation) is significantly better than the ESFs estimated at L = 1 cm and at L = 2 cm. The ESF obtained at 2 cm is further degraded because the beam aperture near the transducer edges is reduced. Compare the ESF curve with the corresponding SF in Fig. 7. Note the close correspondence between the ESF and the SFs estimated at L = 0 and 1 cm, respectively. Lateral signal decorrelation reduces strain sensitivity and dynamic range, as predicted using the SF (Kallel et al. 1997).

CONCLUSIONS

The theoretical predictions of the SF are corroborated using the ESFs in this paper. The contribution of frequency-dependent attenuation is seen in the difference between the ESF in the focal zone and the far-field, respectively. The SNR_e in the elastogram and the sensitivity deteriorate with depth, due to the corresponding reduction in the SNR in the RF signals. In addition, the shift in the ESF toward higher strains with increased depth in the phantom also validates the SF results.

Lateral signal decorrelation reduces the SNR_e, strain sensitivity and dynamic range, as predicted using the SF. The ESFs obtained at different lateral positions in this paper corroborate the SF results. The optimal ESF is, therefore, obtained in the focal zone of the transducer and the axis of symmetry of the phantom (A-line 50), where only the contributions due to axial signal decorrelation are present. The ESF deteriorates with lateral position in the elastogram, due to the lateral motion of tissue scatterers and with depth, due to frequency-dependent attenuation.

Acknowledgements—This work was supported in part by NIH program project grant P01-CA64597 to the University of Texas. The phantom used in this paper was supplied courtesy of Dr. Timothy Hall from the University of Kansas.

REFERENCES

Alam K, Ophir J, Varghese T. Elastographic axial resolution criteria: An experimental study. IEEE Trans Ultrason Ferroel Freq Cont 2000;47(1):304–309.

Bamber CJ, Bush LN. Freehand elasticity imaging using speckle decorrelation rate. Acoustic Imaging 1996;22:285–292.

Bohs LN, Trahey GE. A novel method for angle independent ultrasonic imaging of blood flow and tissue motion. IEEE Trans Biomed Eng 1991;38:280–286.

Céspedes EI. Elastography: Imaging of biological tissue elasticity. Ph.D dissertation. University of Houston, 1993.

Chaturvedi P, Insana M, Hall TJ. 2D companding for noise reduction in strain imaging. IEEE Trans Ultrason Ferroel Freq Cont 1998; 45(1):179–191.

deKorte CL, Céspedes EI, Van der Steen AFW, Lancee CT. Intravascular elasticity imaging using ultrasound: Feasibility studies in phantoms. Ultrasound Med Biol 1997;23(5):735–746.

Gao L, Parker KJ, Lerner RM, Levinson SF. Imaging of the elastic properties of tissue—A review. Ultrasound Med Biol 1996;22(8): 959–977.

Garra BS, Céspedes EI, Ophir J, Spratt RS, Zuurbier RA, Magnant CM, Pennanen MF. Elastography of breast lesions: Initial clinical results. Radiology 1997;202:79–86.

Hall TJ, Bilgen M, Insana MF, Krouskop TA. Phantom materials for elastography. IEEE Trans Ultrason Ferroel Freq Cont 1997;44(6): 1355–1365.

Kallel F, Varghese T, Ophir J, Bilgen M. The nonstationary strain filter in elastography, Part II Lateral and elevational decorrelation. Ultrasound Med Biol 1997;23(9):1357–1369.

Kallel F, Ophir J. Three dimensional tissue motion and its effects on image noise in elastography. IEEE Trans Ultrason Ferroel Freq Cont 1997;44:1286–1296.

Konofagou EE, Ophir J. A new elastographic method for estimation and imaging of lateral displacements, lateral strains, corrected axial strains and Poisson's ratios in tissues. Ultrasound Med Biol 1998; 24(8):1183–1199.

Krouskop TA, Vinson S, Goode B, Dougherty D. A pulsed Doppler ultrasonic system for making noninvasive measurements of the mechanical properties of soft tissue. J Rehabil Res Dev 1987;24: 1–8.

O'Donnell M, Skovoroda AR, Shapo BM. Measurement of arterial wall motion using Fourier based speckle tracking algorithms. Proceedings of the 1991 IEEE Ultrasound Symposium 1991:1101–1104.

Ophir J, Alam KA, Garra B, Kallel F, Konofagou EE, Krouskop TA, Varghese T. Elastography: Ultrasonic estimation and imaging of the elastic properties of tissues. Proceedings of the Institution of Mechanical Engineers, Part H. J Eng Med 1999;213:203–233.

Ophir J, Céspedes EI, Ponnekanti H, Yazdi Y, Li X. Elastography: A quantitative method for imaging the elasticity of biological tissues. Ultrasonic Imaging 1991;13:111–134.

Parker KJ, Huang SR, Musulin RA, Lerner RM. Tissue response to mechanical vibrations for sonoelasticity imaging. Ultrasound Med Biol 1990;16:241–246.

Parker KJ, Lerner RM, Waag RC. Comparison of techniques for *in vivo* attenuation measurements. IEEE Trans Biomed Eng 1988;35(12): 1064–1067.

Varghese T, Ophir J. A theoretical framework for performance characterization of elastography: The strain filter. IEEE Trans Ultrason Ferroel Freq Cont 1997a;44(1):164–172.

Varghese T, Ophir J. The nonstationary strain filter in elastography, Part I Frequency dependent attenuation. Ultrasound Med Biol 1997b;23(9):1343–1356.

Varghese T, Ophir J. Method for the experimental characterization of the noise performance of elastographic systems. Ultrasonic Imaging 1999;21:17–30.

Varghese T, Bilgen M, Ophir J. Multiresolution imaging in elastography. IEEE Trans Ultrason Ferroel Freq Cont 1998;45(1):65–75.

Wilson LS, Robinson DE. Ultrasonic measurement of small displacements and deformations of tissue. Ultrasonic Imaging 1982;4:71–82.

Yamakoshi Y, Sato J, Sato T. Ultrasonic imaging of internal vibration of soft tissue under forced vibration. IEEE Trans Ultrason Ferroel Freq Cont 1990;37(2):45–53.